Modeling of CNT based composites: Numerical Issues

N. Chandra, and C. Shet
FAMU-FSU College of Engineering, Florida State University, Tallahassee, FL 32310

Introduction

The excellent mechanical properties exhibited by CNTs (Young's modulus are in the range of 0.32 to 1.47 TPa [1,2,3] and failure strength is of the order of 150 GPa [3]) and combined with their extremely high strength to weight ratio make them potential candidates as reinforcing fibers in super strong composites. A critical issue in the successful application of these composites is the mechanical characteristics of fiber-matrix interfaces. Interfaces are narrow regions separating well-defined domains and are primarily responsible for a range of key properties including stiffness, strength, and fracture behavior [4]. The role of interface is very vital to the stress transfer between the fiber and matrix; and the interfaces influence mechanical performance and fracture behavior of the composites under various loading conditions [5].

In the past interfaces have been modeled as a narrow region of continuum with graded properties, or as an infinitely thin surface separated by springs, and cohesive zones with specific traction-separation relations. Chandra et al, [6,7,8] simulated the interfacial mechanical behavior of thin-slice push-out tests incorporating the spring layer model and fracture mechanics approach. In recent years, interfaces are modeled using cohesive zone approaches, which cannot only model interface-bonding behavior, but also its separation without use of any ad-hoc criterions. CZM was originally proposed by Barenblatt [9] as a possible alternative to the concept of fracture mechanics in perfectly brittle materials. In a general CZM the traction-separation relations for the interfaces are such that with increasing interfacial separation, the traction across the interface reaches a maximum, then decreases and eventually vanishes, permitting a complete decohesion. The shape of traction-separation equations, the maximum traction, σ_{max}, and corresponding δ_{max}), and the value of δ_{sep} affects the macroscopic mechanical response of a material system.. Usually the $T-\delta$ relation is expressed in the form of T_n vs. u_n/δ. The normalizing (u_n/δ) is necessitated by the requirement that when traction is obtained as a function of cohesive strength, the multiplier has to be a non-dimensional quantity. It should be noted that δ varies anywhere from 10^{-10} m to 10^{-5} m and σ_{max} ranges from MPa to GPa.

In this paper we model CNT based composite material system in a multiscale set up, where we use the nanoscopic material properties obtained from MD simulations in to a continuum model. In nano-composites interface plays a crucial role, hence nanoscopic

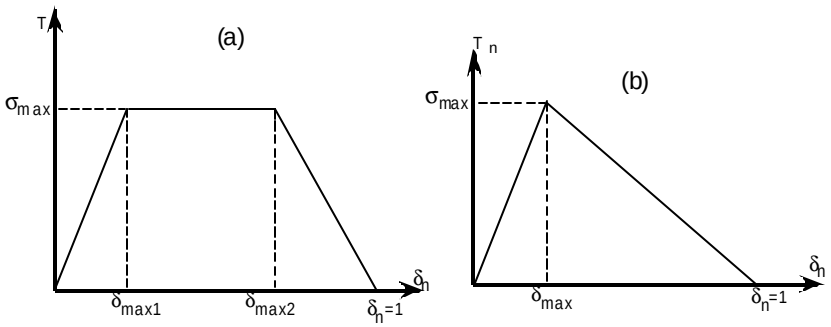

Fig.1 Traction-displacement curve (a) Trapezoidal model for shear traction (b) bilinear model for normal

properties of interface are incorporated in the continuum model through CZM. The continuum model we use in our simulation is FEM. Both CNT and matrix material are modeled using continuum element, where the CNT elements are treated as elastic, while matrix material is treated as elasto-plastic material. In order to predict accurate behavior of the composites appropriate FE mesh has to be adopted. The nanoscopic material properties of the interface sometimes determine the mesh size of elements that need to be adopted near the interface. As reported in the literature [10] the size of the cohesive zone element should be of the order of characteristic distance parameter. By adopting such a mesh density, to model a composite of few mm sizes, we may need elements in several thousands. Here we explore the optimum size needed for cohesive zone elements so that we can use lesser elements to model the composite.

Cohesive Zone Model for Interfaces

The interfacial constitutive relations for the interfaces is approximated by a trapezoidal model of Tevergaard [11] for tangential separation and bilinear model for normal separation This traction-displacement relations are obtained with out any potential and the shape of the traction displacement is trapezoidal as shown in the figure 1.

$$T_t = \begin{cases} \dfrac{\sigma_{max}}{\delta_{max1}} \cdot \delta_t, (\delta \le \delta_{max1}) \\ \sigma_{max}\,(\delta_{max1} \le \delta \le \delta max2) \\ \dfrac{\sigma_{max}}{\delta} \cdot \dfrac{1-\delta}{1-\delta_{max}} \cdot \delta_t, (\delta > \delta_{max2}) \end{cases} \quad ; \; T_n = \begin{cases} \dfrac{\sigma_{max}}{\delta_{max1}} \cdot \delta_n, (\delta \le \delta_{max1}) \\ \dfrac{\sigma_{max}}{\delta} \cdot \dfrac{1-\delta}{1-\delta_{max}} \cdot \delta_n, (\delta > \delta max1) \end{cases} \tag{1}$$

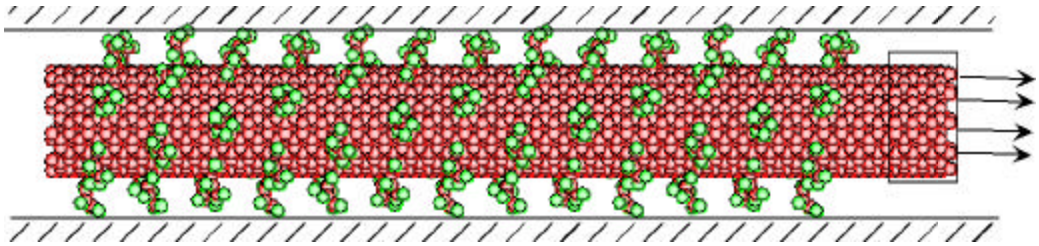

Fig.2 Schematic of (10,10) CNT with butane hydrocarbon chemical attachments.

Interface Properties from MD Simulation

Interface properties were obtained by simulating fiber pullout experiment using MD simulations. Here a (10,10) nanotube of 120 $\mathring{A}$ length is considered in the investigation. Hydrocarbon chains are attached to the nanotubes at randomly selected positions through the length of the nanotube. Tensile stresses are applied by displacing one end of the nanotube while fixing the corner atom of hydrocarbon chain as shown in figure 2. Displacements of 0.05 A are applied every 1000 time steps with a step size of 0.2 fs. Temperature is maintained at 300K. Stresses strains and reactions of fixed atoms are monitored. A typical Reaction force vs displacement plot for fixed atoms is shown in figure 3. There is an initial flat region which corresponds to stretching of hydrocarbon chains. This is followed by a rise and drop which denote bonding and de-bonding, and a final detachment of the tube.

The most interesting aspect of interface behavior is the bonding and de-bonding of nanotube interfaces. The sliding of hydrocarbon chains along the nanotube before failure

is responsible for this behavior. Using such force-displacement data from simulation, traction displacement curves are obtained in the format of CZM model indicated by figure 1 and Eq. 1.

CZM based shear lag model

In this section we propose an analytical model based on shear lag model concept originally proposed by Cox [12] and Kelly [13]. In most of the shear lag models the fiber and matrix at the interface is considered to be perfectly bonded. But in reality it is difficult to achieve a near perfect bonding between the fiber and matrix. The interface starts separating with applied loading. In the present analytical model we incorporate the interface separation by including cohesive zone model. For a composite where the fibers are of uniform length and diameter and fibers are aligned in a matrix, a unit cell as shown in the fig. 4(b) is identified for the analytical and numerical analysis. Let the tensile strain on composite be e in the z direction. Let E_f, s_f and t_f be the Young's modulus, longitudinal stress and shear stress in the fiber, T_s be the interfacial shear traction, u, v be the axial displacement in the fiber and surrounding matrix respectively. The difference in axial displacements, $u_f^+ - v_m^-$ is the displacement jump between the interface between fiber and matrix inducing the interfacial shear traction T_s. The longitudinal and shear stress in the fiber is given by

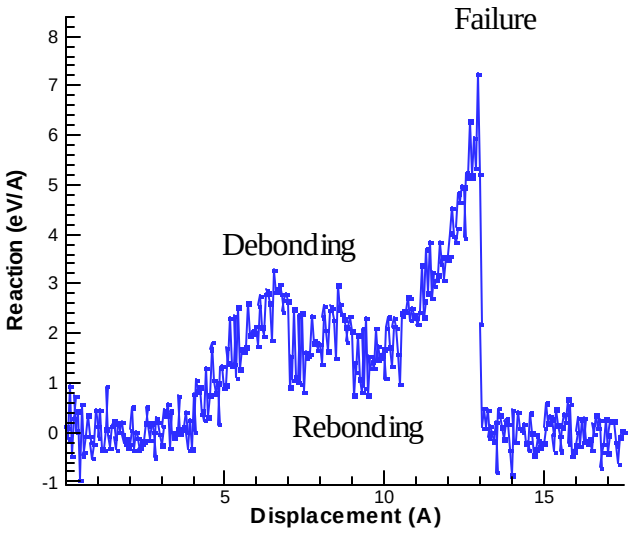

Fig 3. Schematic of force-displacement behavior of interface obtained from MD calculations. This is the basis for traction-displacement plot for cohesive zone model

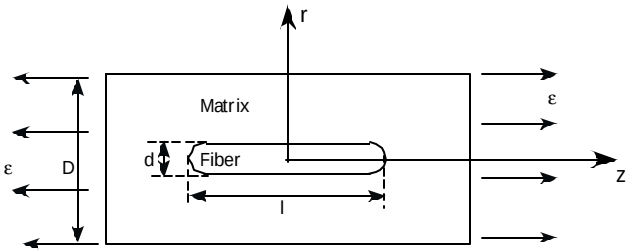

Fig. 4. Shear lag model for aligned short fiber composites.

$$s_f = E_f e\left[1+\frac{\left(\frac{s_o}{E_f e}-1\right)\cosh(b z)}{\cosh\left(b l/2\right)}\right]; \quad t_f(z) = \frac{E_f e d}{l\cosh\left(b l/2\right)}\left[\left(\frac{s_o}{E_f e}-1\right)(1. - \cosh(b z))\right] \quad (2)$$

The average stress in the fiber can be calculated as

$$\bar{s}_f = \frac{2}{l}\int_0^{l/2} s_f dz = E_f e\left[1+\frac{\left(\frac{s_o}{E_f e}-2\right)\tanh\left(b l/2\right)}{\left(b l/2\right)}\right] \quad (3)$$

Defining the average stress in matrix as $\bar{s}_m = E_m e$, where E_m is the Young's modulus of the matrix and V_f is the volume fraction of fiber in the composite then the average stress in composite is given by $s_c = (1 - V_f)\bar{s}_m + V_f \bar{s}_f$. If E_c is the Young's modulus of the composite, then we can write $s_c = E_c e$.

FE model

To evaluate the mechanical behavior of composites, the unit cell is modeled as an axi-symmetric problem. The CNT is modeled as a hollow tube with a length of 200 Å, outer radius of 6.98 Å and thickness of 0.4 Å. The CNT tube was discretized with 1596 axisymmetric 4-node elements and 11379 axisymmetric 4-node elements to model the matrix. Duplicate nodes are created at the interface on the fiber and matrix sides. 399 axisymmetric cohesive elements with each having 4 nodes and zero thickness in the direction normal to the interface are used to model the interface behavior. Symmetric boundary conditions were used along the axis of symmetry. The cohesive element model is input as a user-defined element subroutine UEL into general-purpose commercial code ABAQUS to carry out the analysis. The model was simulated by applying tensile displacement on the top edge of unit model. Cohesive zone properties were applied to interface elements with T_{max} varying between 50 to 5000 MPa. Interface bonding along the curved cap of CNT is ignored by reducing the interface strength.

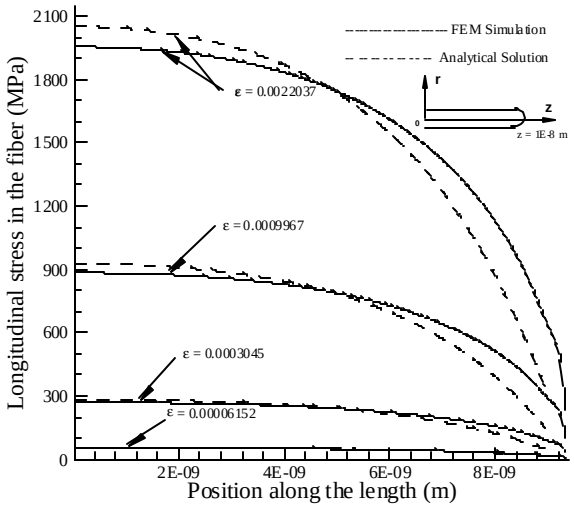

Fig. 6 Variation on longitudinal stress in the fiber at different applied strain levels in the composite, for T_{max}=5000Mpa.

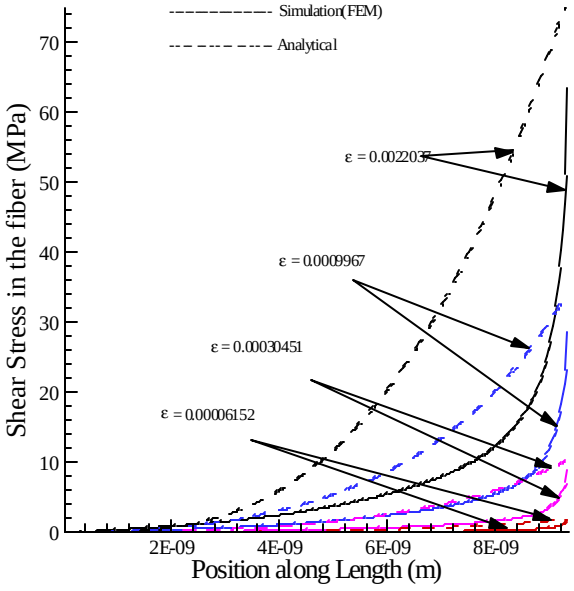

Fig. 7 Variation on Shear stress in the fiber near the interface at different applied strain levels in the composite, for T_{max}=5000MPa.

Results and discussions

Variation of Longitudinal stress and shear stress in the fiber:

Figure 6 shows the variation of longitudinal stress and figure 7 shows the variation of shear stress in the fiber for interface strength T_{max}=

5000 MPa. Plots with solid lines are obtained from FEM simulations and plots with dashed lines are obtained from analytical solution (Eq. 2). There is a good comparison for longitudinal stresses between numerical model and analytical model for interface strengths of 5000 as shown in figure 6 The shear stress distribution from the two models deviate from one another. However the maximum intensity of shear stress predicted by the two models compare with in a close range, for e.g. the maximum shear stress predicted for the strain level of 0.0022 is 68 MPa and 74 MPa by numerical and analytical models respectively for the interface strength of 5000 MPa.

Effect of interface strength on stiffness and strength:

It has been observed in the literature that composite strength and stiffness increase with matrix stiffness and volume fraction of fiber. Table 1 and the stress strain curves shown in the figures 8 and 9 show that that the strength and stiffness also increases with interface strength. For example for Epoxy matrix (E=3.5 GPa) the stiffness in the elastic range increases by a factor 11 when the interface strength is 5000 MPa and volume fraction is 0.05%, on the other hand with weak interface strength of 50 MPa the stiffness increases by a factor 0.5. In addition to stiffness the strength also increases considerably. For example for composite with volume fraction of 0.05%, the yield strength (when matrix reaches a yield strain of 0.0216) are of the order 107, 340, and 809 MPA for interface strength of 50, 500 and 5000 MPa respectively.

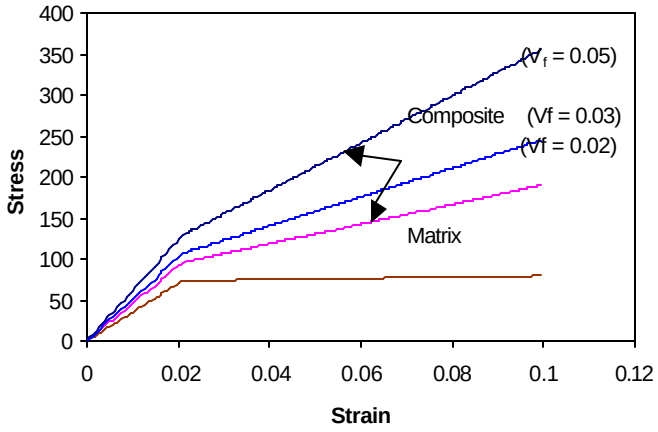

Fig. 8. Stress strain curve for E-glass-composite for different volume fraction of fiver and for interface strength of 500 MPa

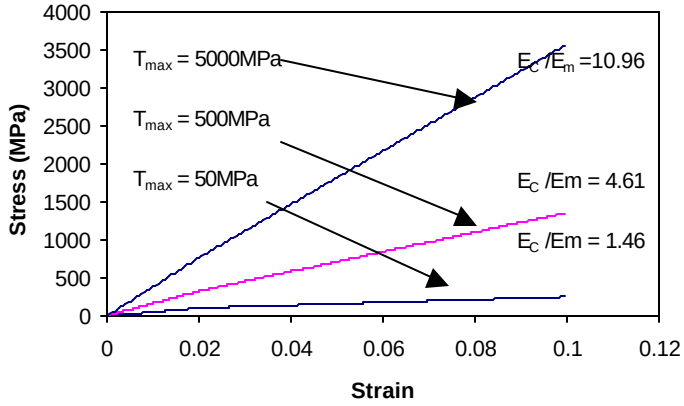

Fig. 9 Stress strain curve for CNT based-composite for different interface strength and volume fraction of 0.05

Effect of interface strength on Hardening modulus:

Higher interface strength also tends to increase hardening modulus of composites. Table 3 below shows the different range of hardening modulus attained with different interface strength. In case of conventional composite consisting of E-glass (E=76 GPA) and Epoxy matrix there is marginal increase of hardening modulus. This is because the stiffness of the fiber is very low. In such cases the matrix material governs the mechanical behavior once composite reaches its yield value. In case of CNT based composites with low

interface strength there is no considerable increase in hardening modulus. Even though the fiber is considerably stronger, matrix controls the composite behavior. On the other hand with stronger interface there is considerable increase in hardening modulus as shown in table 3 and Figures 13,14 and 15. In case of interface strength of 5000 MPa, with 0.05 % volume fraction of fiber, the hardening modulus is 90% of that of elastic stiffness. With stronger interface and stronger fiber stiffness, mechanical behavior is controlled by fiber where as in composites with low interface strength or low fiber stiffness matrix governs the composite behavior.

Volume fraction of fiber	Interface strength T_{max} (in MPa)	CNT/Epoxy Composite		E glass/Epoxy Composite	
		E_c(elastic)/E_m	E_c(Hardening)/E_m	E_c(elastic)/E_m	E_c(Hardening)/E_m
0.02	50	1.18	0.2	1.11	0.16
	500	2.46	1.49	1.3	0.34
	5000	4.98	4.02	1.38	0.42
0.03	50	1.28	0.32	1.17	0.22
	500	3.17	2.22	1.45	0.61
	5000	6.99	6.02	1.57	0.74
0.05	50	1.46	0.53	1.29	0.35
	500	4.61	3.68	1.75	0.93
	5000	10.96	10.02	1.95	1.23

Table 1: Variation of Young's modulus and hardening modulus of the composite with matrix young's modulus, volume fraction and interface strength

References

[1]. M.F. Yu, B.S. Files, S. Arepalli and R.S. Ruoff, Phys. Rev. Lett. 84 (2000) 5552.

[2]. A. Krishnan, E. Dujardin, T.W. Ebbesen, P.N. Yianilos and M.M.J. Treacy, Phys. Rev. B, 58. pp. 14013-14019, 2001.

[3]. B.G. Demczyk, Y.M. Wang, J. Cumings, M. Hetman, W. Han, A. Zettl and R.O. Ritchie, Mater. Sci. and Eng. A 334 (2002) 173.

[4]. Jayaraman, K., K.L. Reifsnider and R.E. Swain, (1993) Journal of Composites Technology and Research 15(1), 14-22.

[5]. Kim, J.K. and Mai, Y.W. (1991a) *Composites Sci. Technol.* 41, 333-378.

[6]. Ananth, C.R. and Chandra, N., (1995a) *Mech. Compos. Mater. Struct* 2, 309-328.

[7]. Ananth, C.R. and Chandra, N., (1995b) *J. Compos. Mater.* 29, 1488-1514.

[8]. Chandra, N. and Ananth, C. R., (1995c) *Compos. Sci. Technol* 54, 87-100.

[9]. Barenblatt, G.I.,(1959) *PMM*, vol.23, 434-444.

[10]. Camacho, G.T. and Ortiz, M. (1996) *Int. J. Solids Structures* 33, 2899.

[11]. Tvergaard, V. (1990) *Mater. Sci . Eng. A*125, 203.

[12]. Cox, H.L. (1952), J. Appl. Phys., Vol. 3, p. 72

[13]. Kelly, A., (1973), Strong Soilids, 2nd Ed., Oxford University Press, Chap. 5.